Journal of Materials Chemistry B

Accepted Manuscript

ROYAL SOCIETY OF CHEMISTRY

www.rsc.org/materialsB

Journal Name Journal of Materials Chemistry B Dynamic Article Links ►

Cite this: DOI: 10.1039/c0xx00000x

www.rsc.org/xxxxxx

ARTICLE TYPE

Surface charge-reversible polyelectrolyte complex nanoparticles for hepatoma-targeting delivery of doxorubicin

Xubo Zhao[a], Peng Liu[a,*], Qilei Song[a], Nan Gong[a], Liangwei Yang[a] and Winston Duo Wu[b]

Received (in XXX, XXX) Xth XXXXXXXXX 20XX, Accepted Xth XXXXXXXXX 20XX

DOI: 10.1039/b000000x

Polymeric nanoparticles are greatly advancing the field of nanomedicine due to their ability for targeted and controlled drug release. Here, monodisperse pH-responsive surface charge-reversible and hepatoma-targeting polyelectrolyte complex nanoparticles (GC/HA NPs) near 80 nm were prepared via the ionotropic gelification by simple and mild co-precipitation of the galactosylated chitosan (GC) and hyaluronate (HA). Their surface charges could transfer from negative in neutral or basic media to positive in acidic media, indicating their potential application for delivering anti-tumor drugs in response to the extracellular pH of the tumor environment. The unique "electrostatic sponge" structure enhanced their drug-loading capacity and encapsulation efficiency towards the anti-cancer doxorubicin (DOX), as well as the pH-triggered controlled release. MTT assays and fluorescence microscope analysis revealed that the DOX-loaded GC/HA NPs possessed the hepatoma-targeting capacity with favorable biocompatibility. These features make them advanced anti-cancer drug nanocarriers for intelligent drug delivery system.

1. Introduction

The stimuli-responsive drug release system (DDS) has been extensively investigated for controlled drug delivery due to the physiological differences of various tissues. Compared with the normal tissues, the tumor tissues possess a variety of physicochemical properties and unique micro-structural features. Typical biological properties exploited for anti-cancer drug delivery include abnormal temperature gradients,[1] over expressed proteins and enzymes,[2] hypoxia,[3] weak acidity,[4] and vascular abnormalities.[5] Especially, the intracellular microenvironment of the tumor tissues exhibits acidic pH inside endosomes and lysosomes (pH 4.5–6.5), which could be utilized to modulate and trigger anti-cancer drug release profiles.[6]

In recent years, one of the critical challenges in medical diagnosis and therapy is to develop physicochemical properties triggering the on-demand release of the anti-cancer drugs in intracellular microenvironment of the tumor tissues. Thus many efforts have been devoted to develop stimuli-responsive nanocarriers for controlled drug delivery. The typical biological stimuli exploited for triggering drug release include pH[7-9] and temperature differences,[10,11] redox media,[12,13] enzymes,[14,15] and neurotransmitter.[16] Among these stimuli,[17] pH-responsiveness has been mainly developed for anti-cancer DDS in the past decades. Meantime, external stimuli were also utilized as available tools for triggering drug release, such as near-infrared light.[18]

Furthermore, the surface charge of the nanocarriers is the key parameter for DDS to control *in vivo* fate.[19] It is expected that the surface charge of the pH-responsive drug nanocarriers changes from negative to positive, as the pH values change from basic or neutral in body circulation to slightly acidic in the drug release environment. The negative-charged nanocarriers exhibit a prolonged circulation time in blood circulation, and prevent from swallowing by the reticuloendothelial system (RES).[20-22] However, the positive-charged nanocarriers show higher affinity to the negative-charged cell membranes and thus can be readily internalized by the cells.[20,21] Therefore, the DDS for anti-cancer drugs based on the surface charge-reversal strategy can maintain their stealth character during blood circulation and promote cellular uptake, spontaneously and precisely triggering responsive release or enhance interaction between nanocarriers and cells at the targeting disease sites.[7,23]

Besides the surface charge of the drug-carriers, their size also plays an important role in overcoming the RES barriers to deliver chemotherapeutic drugs deeply into the tumor by means of intravenous injection.[24-26] The discontinuous endothelium of tumor blood vessels forms many pores ranging in size from 200 nm to 2 μm with the average pore size of 400 nm on the vessel walls, the nanoparticles with size smaller than 200 nm are thus favorable for extravasation from blood stream into tumors through the enhanced permeability and retention (EPR) effect.[27,28] So the nanoscaled drug delivery vehicles have recently attracted considerable attention.

It is well-known that most anti-cancer drugs have serious side effects due to their unspecific actions on normal tissues. By utilizing antibodies or specific ligands, the drug delivery vehicles along with the therapeutic agents can selectively bind to the targeting-cells, and then be delivered to the interior of a given type of cells via the receptor mediated endocytosis.[29] Among various targeting ligands, the galactose moiety with very high

affinity to the galactose receptors (ASGP-R (asialoglycoprotein)) on the hepatocyte surface, could be efficiently bound and internalized by the ASGP-R over-expressing cells.[30,31] Therefore, conjugating galactose group to nanocarriers has been used to design novel tumor-specific delivery vehicles.

In the present work, all the characteristic features abovementioned for the intelligent delivery of anti-cancer drugs have been integrated in the form of the galactosylated chitosan /hyaluronate polyelectrolyte complex nanoparticles (GC/HA NPs), prepared via a simple and mild ionotropic gelification technique (Scheme 1). Besides the biocompatibility, surface charge-reversal, pH-triggered controlled release and hepatocyte-specificity features, the unique "electrostatic sponge" structure of the polyelectrolyte complex nanoparticles possessed high DOX encapsulation efficiency and loading capacity.

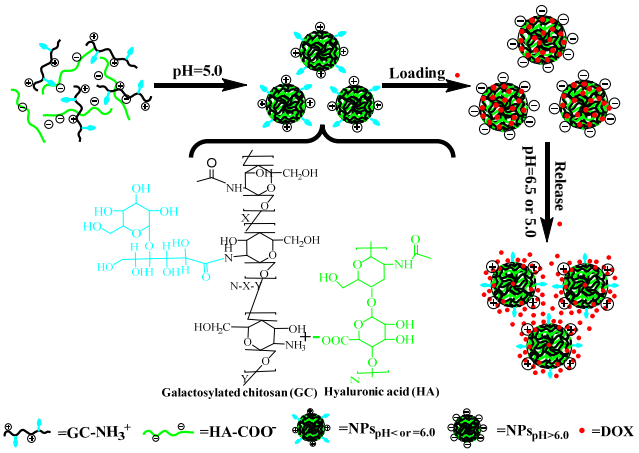

Scheme 1 Schematic illustration of the preparation, ideal structural transformation and drug release of the GC/HA NPs.

2. Experimental Section

2.1. Materials and reagents

Chitosan (CS, viscosity-average molecular weight of 50k or 100k and N-deacetylation degree of 95%) was purchased from Yuhuan Ocean Biochemical Co. Ltd. Sodium hyaluronate (HA, MW of 240 000) was purchased from Shandong Freda Biopharm Co. Ltd. Lactobionic acid (LA) was purchased from Gracia Chemical Technology Co. Ltd. 1-Ethyl-3-(3-dimethyl aminopropyl) carbodiimide hydrochloride (EDC•HCl) was purchased from Fluorochem. N-hydroxylsuccinimide (NHS) was purchased from Aladdin Chemistry Co. Ltd. N,N,N'N'-tetramethylethylenediamine (TEMED) was supplied by Aldrich (WI, USA). Doxorubicin hydrochloride (DOX) was purchased from Beijing Huafeng United Technology Co. Ltd. All other reagents were analytical reagent grade purchased from Tianjin Chemical Company. Deionized water was used throughout.

2.2. Synthesis of GC

Coupling of LA with chitosan was performed using EDC·HCl and NHS as coupling agents.[31] Briefly, 0.1911 g (0.5333 mmol) LA, dissolved in 50 mL TEMED/HCl buffer solution (pH 4.7), was activated with a mixture of NHS (0.0307 g) and EDC (0.1022 g). Subsequently, 1.0003 g chitosan (5.5901 mmol with relative molecular weight around 100k) was added into the solution. The reaction was performed for 72 h at room temperature. The resulting product was purified using a dialysis tube (12,000 MWCO) against distilled water for 4 days, followed by lyophilization and stored at 4 °C.

Another GC was also prepared by the above mentioned procedures with chitosan of relative molecular weight of 50k.

2.3. Preparation of GC/HA nanoparticles

The co-precipitation method was used to prepare the GC/HA NPs by the electrostatic interaction between the amino groups of the GC and the carboxyl groups of HA as following (Table 1): GC prepared from CS with relative molecular weight of 50k or 100k (GC_{50} or GC_{100}) was dissolved into 0.10 mol/L acetic acid aqueous solution. HA solution was prepared by dissolving sodium hyaluronate in deionized water. After the pH values of the GC and HA solutions were adjusted to 5.0, they were stirred for 24 h, and filtered with filter paper to remove any un-dissolved substances.

After 100 mL GC solution was dropped into 100 mL HA solution with a rate of 3 drops per second under stirring at 400 rpm, the mixture was stirred for another 8 h. Finally, the GC/HA NPs were separated by centrifugation and washing twice with deionized water.[32]

For comparison, the CS/HA NPs were also prepared with CS as the polycation via the above procedure.

Table 1. Experimental conditions for the GC/HA NPs.

Samples	M_{vGC}	C_{GC} (g/mL)	C_{HA} (g/mL)	Diameter (nm) [a]	Diameter (nm) [c]
NP-1	50k	0.05	0.0571	88.54±21.90	136
NP-2	50k	0.10	0.1143	95.72±16.32	167
NP-3	50k	0.15	0.1714	94.83±38.52	194
NP-4	100k	0.05	0.0571	68.55±16.67	113
NP-5	100k	0.10	0.1143	83.12±9.60	128
NP-6	100k	0.15	0.1714	90.69±30.44[b]	209
NP-7	100k	0.10	0.1143	23.46±4.65[b]	43

[a] Measured by TEM through calculating from 200 particles.
[b] Irregular nanoparticles or aggregation.
[c] presented hydrodynamic diameter by DLS.

2.4. Drug loading and controlled release

10 mg GC/HA NP-5 were added into 5.0 mL DOX solution (1.00 mg/mL, pH 7.4) for the drug-loading. After being stirred for 24 h and swung subsequently by table concentrator for 24 h, the DOX-loaded GC/HA NP-5 were centrifuged to remove the excess DOX. Then, the drug concentration in the supernatant solution was analyzed using an ultraviolent (UV) spectrophotometer at 480 nm to assess the drug-loading capacities. The DOX-loading capacity and encapsulation efficiency of the GC/HA NP-5 were calculated from the drug concentrations in solution before and after adsorption.

The DOX-loaded GC/HA NPs were re-dispersed into 10 mL phosphate-buffered saline (PBS) with different pH values, transferred into dialysis tubes with a molecular weight cutoff of 14,000, and immersed into 120 mL PBS at 37 °C under a certain pH value, respectively. 5.0 mL of aliquot was taken out at certain time intervals, and then the drug concentration in the dialysate was analyzed using UV-vis spectrometry at 480 nm to calculate the cumulative release, as the total percentage of drug molecules released through the dialysis membrane over time. 5.0 mL of

fresh PBS was added after each sampling to keep the total volume of the solution constant.

The *in vitro* drug release data were analyzed for the release mechanism, using the Higuchi[33] and Korsmeyer-Peppas[34] drug release equations.

2.5. Cell toxicity and hepatocyte-specificity assays

MTT (3-(4,5-dimethylthiazol-2-yl)-2,5-diphenyltetrazolium bromide) assay was performed to evaluate the cytocompatibility and hepatocyte-specificity of the GC/HA NPs to HepG2 cells, with DOX as the model drug to evaluate the hepatocyte-specificity. After the cells seeded in a 96-well cell culture plate at a density of 1×10^5 cells per well were cultured in 5% CO_2 at 37 °C for 24 h, different concentrations of the GC/HA NP-5, the DOX-loaded GC/HA NP-5, DOX-loaded CS/HA NPs in the presence of 1 mM lactobionic acid or free DOX was added and incubated for 24 h. Then the cells were washed three times with PBS and processed for the MTT assay. 100 μL PBS (pH 7.4) containing 20 μL of MTT (5 mg/mL) solution was added to each well, and incubated for 4 h. After the cell bound dye was dissolved with 100 μL DMSO and swung by table concentrator for 20 min, the absorbance of each well was read on a microplate reader at 490 nm.

2.6. Fluorescence microscope analysis

The cellular release of DOX from the DOX-loaded GC/HA NP-5 in the absence or presence of 1 mM free lactobionic acid as determined by fluorescence microscope (Olympus BX43) using HepG2 cells after 12 h incubation. Furthermore, excitation wavelengths of 405 nm for Hoechst and 480 nm for DOX were utilized to validate the location fluorescence.

2.7. Characterizations and measurements

Nicolet Satellite infrared spectrometer was used for the FT-IR spectroscopy analysis in the range of 400-4000 cm^{-1} with the resolution of 4 cm^{-1}, by the KBr pellet technique.

^{1}H-NMR spectra were recorded with a 400 MHz spectrometer (Bruker, Advance 400 MHz) at room temperature. The mixture of D_2O/acetic acid-D_4 (v/v of 12:1) was used as a solvent.

Elemental analysis of C, N and H of the GC/HA NP-5 was performed on an Elementar vario EL instrument (Elementar Analysensysteme GmbH).

The zeta potentials of the same concentration GC/HA NP-5 in media of various pH values were determined using a Zetasizer Nano ZS (Malvern Instruments Ltd.).

The morphologies of the polyelectrolyte complex nanoparticles prepared under different conditions were characterized with a JEM-1200 EX/S transmission electron microscope (TEM) (JEOL). They were dispersed in water in an ultrasonic bath for 5 min, and then deposited on a copper grid covered with a perforated carbon film.

The mean hydrodynamic diameter and size distribution of the polyelectrolyte complex nanoparticles were determined by the dynamical mode (DLS) on the Light Scattering System BI-200SM, Brookhaven Instruments device equipped with the BI-200SM goniometer, the BI-9000AT correlator, temperature controller, and the Coherent INOVA 70C argon-ion laser at 20 °C. DLS measurements were performed using 135-mW intense laser excitation at 514.5 nm and at a detection angle of 90° using the dispersion directly at 25 °C.

The drug-loading and controlled release performance of the GC/HA NP-5 were assessed using a Perkin-Elmer Lambda 35 UV-vis spectrometer (PerkinElmer Instruments) at room temperature.

3. Results and Discussion

3.1. Preparation of GC/HA NPs

GC was synthesized as the polybase for the preparation of the polyelectrolyte complex nanoparticles. In the ^{1}H NMR spectrum of GC (Figure 1), the chemical shifts at δ =4.05 ppm (b) and 4.13 ppm (a) are assigned to the characteristic protons of LA. Herein, the substitution values of LA in GC could be calculated, based on the area ratio of signals at 4.05 ppm (b) and 4.13 ppm (a) and that of 2.01 ppm peak attributed to the original acetamide group of chitosan. The substitution values of galactose coupled with chitosan 100 k and 50k are 6.82–7.27% and 5.91-6.13% of the total amine functions in chitosan. The optimal substitution values of galactosylation was reported to be about 5%, which shows the high transfection in human hepatocyte-derived cell lines (HepG2).[30,35] So the GCs (50k and 100k) are expected to exhibit the hepatoma-targeting function.[25]

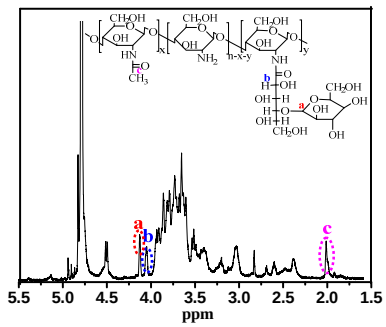

Figure 1. ^{1}H NMR spectrum of GC (100 k) (400 MHz) in D_2O/acetic acid-D_4.

The polyelectrolyte complex nanoparticles were prepared by a simple and mild co-precipitation method, via the electrostatic interaction between the polybase (GS) and the polyacid (HA). A light-blue color due to light-scattering by the minute suspended particles (Tyndall effect) was observed at the beginning of co-precipitation after 8 mL GC solution had been dropped into the HA solution.[36] The morphology and size of the GC/HA NPs were investigated by TEM in dried state and by DLS in aqueous solution at certain pH media, respectively. The effects of the relative molecular weight of CS and the feeding ratio of HA and GC on the polyelectrolyte complex nanoparticles are summarized in Table 1.

The TEM images of the polyelectrolyte complex nanoparticles prepared under different conditions are compared in Figure 2. The typical well-defined GC/HA NPs were spherical shape and near monodisperse in size, with average size of 83.12±9.60 nm (Figure 2e). It could be found that the relative molecular weight of GC had limited effect on the morphology and size-distribution of the polyelectrolyte complex nanoparticles. Compared with the

typical NP-5 (Figure 2e), the NP-1 (Figure 2a) and NP-2 (Figure 2b) were of much wider polydispersity in size.

The concentrations of the GC and HA solutions showed remarkable influence on the size and morphology of the GC/HA NPs. However, after certain concentrations of GC and HA were reached, no well-defined GC/HA nanoparticles was obtained because of aggregation (Figure 2c and f).[37,38]

The adding order was found to be the most dominant factor in the formation of the GC/HA NPs. By adding the HA solution into the GC solution, the obtained products (NP-7) presented granulometric state of aggregates (Figure 2g). Based on the investigation above, the well-defined GC/HA NP-5 with monodisperse particle size of 83.12±9.60 nm were chosen for the subsequent experiments.

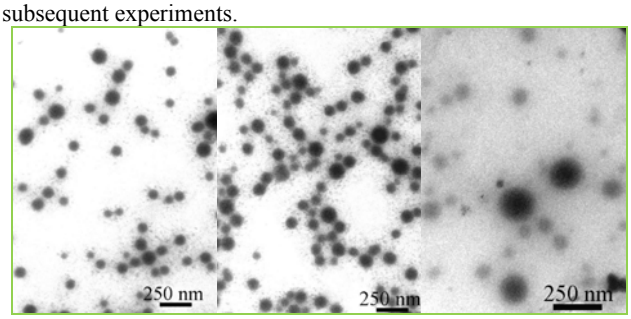

(a) NP-1 (b) NP-2 (c) NP-3

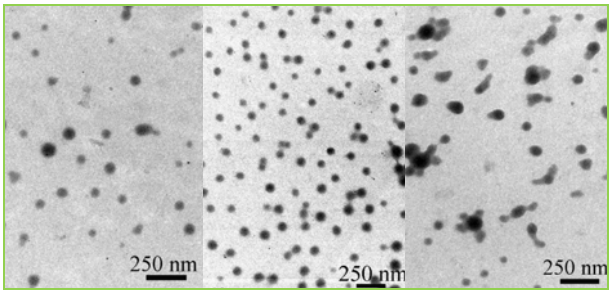

(d) NP-4 (e) NP-5 (f) NP-6

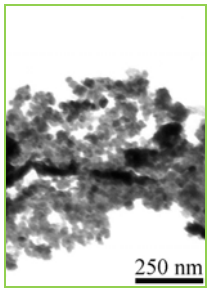

(g) NP-7

Figure 2. The TEM images of the GC_{50k}/HA 0.05 g/100 mL (a, NP-1), GC_{50k}/HA 0.10 g/100 mL (b, NP-2), GC_{50k}/HA 0.15 g/100 mL (c, NP-3), GC_{100k}/HA 0.05 g/100 mL (d, NP-4), GC_{100k}/HA 0.10 g/100 mL (e, NP-5), GC_{100k}/HA 0.15 g/100 mL (f, NP-6), and HA/GC_{100k} 0.05 g/100 mL (g, NP-7).

The chemical components of the GC/HA NP-5 were examined using elemental analysis. The GC content (GC%) in the GC/HA NP-5 was calculated to be 68.03%±1.20% (mean ± standard deviation, n=4) from the N content. The results indicated that the CS content (CS%) was higher the HA content (HA%) in the GC/HA NP-5, although the molar ratio of the amino groups in the GC and the carboxyl groups in HA was controlled at about 0.95:1, due to the substitution values of galactosylation of the GC_{100k} of 4.55%±0.18%. This might be due to the poorer aqueous solubility of GC than HA. Furthermore, some amino groups had been transferred into the un-ionizable amide groups after the galactosylation, further decreasing the solubility of GC and consequently facilitating the precipitation of GC_{100k}, resulting into the NPs 7 aggregates (Figure 2g).

3.2. pH and ionic strength stimuli-responsive properties

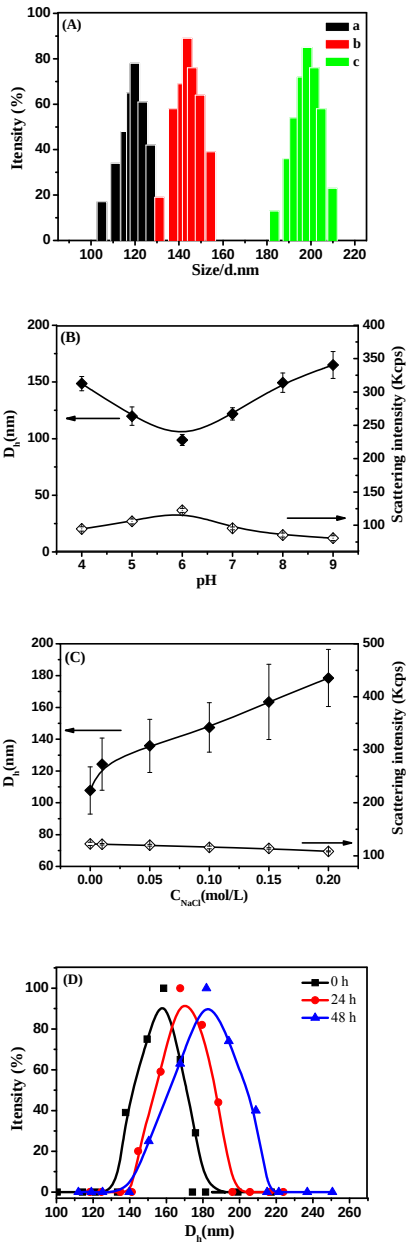

Figure 3. Typical D_h distributions at pH 5.0 of (a) theGC/HA NP-5, (c) DOX-loaded GC/HA NP-5, and (b) DOX-loaded GC/HA NP-5 after drug-releasing at pH 5.0 PBS for 24 h (A), the dependence of the D_h on pH (B) and ionic strength (C) in aqueous media, and typical D_h distribution of the GC/HA NP-5 in normal saline for different times, as measured by DLS. The D_h (nm) and scattering intensity's value are shown (mean ± standard deviation, n=5).

The GC/HA NP-5 displayed a narrow unimodal size distribution with an average hydrodynamic diameter (D_h) of 119 ± 5 nm at pH 5.0, measured using DLS (Figure 3A). The pH dependence of the GC/HA NP-5 was investigated and the results are presented in Figure 3B. The D_h of the GC/HA NP-5 decreased from 148.56±6.28 nm to 98.74±4.85 nm when the media pH value changed from 4.0 to 6.0, and then increased, reaching 164.94±11.93 nm at pH 9.0. Increasing of pH probably weakened the electrostatic interaction between HA and GC, resulting in a decrease of electrostatic interactions within the internal structure of the GC/HA NP-5. The GC/HA NP-5 were smaller between pH 4.0 and 6.0, and their size increased as the pH was increased from 6.0 to 9.0. Furthermore, the D_h of the GC/HA NP-5 emerged the minimal value 98.74±4.85 nm in pH 6.0 media. The phenomenon reveals that the electrostatic interaction between the polyanion and polycation changed in slightly acidic conditions. However, when the media pH was less than 4.0, or higher than 9.0, the structure of the GC/HA NP-5 loosed due to the weakened electrostatic interaction. This may due to the HA moiety of the GC/HA NP-5 becoming more hydrated and extended, or even dissolved, because of its protonation at strong alkaline medium and same trend of the GC moiety at strong acidic medium. On the other hand, the light scattering intensity of the sample only changed slightly when the pH of the medium was increased from 4.0 to 6.0, indicating that the GC/HA NPs had a good structural stability and resistance against pH change.

The effect of the ionic strength on their D_h was also investigated using DLS (Figure 3C). Their D_h increased from 103.8±4.85 nm to 164.94±7.94 nm as the NaCl concentration increased from 0 to 0.20 mol/L. The small molecule electrolyte could weaken both the electrostatic repulsion among the same group and the electrostatic interaction between the amine groups of the GC and the caboxyl groups of HA in the polyelectrolyte complex nanoparticles, due to the shielding effect.[39] Furthermore, the scattering intensity of the polyelectrolyte complex nanoparticles was close to a steady value near 115 Kcps, indicating that the GC/HA NPs did not aggregate within such ionic strength range.

The stability of the GC/HA NP-5 was tracked by DLS analysis as shown in Figure 3D. Their hydrodynamic diameter (D_h) increased slightly with increasing of dispersing time from 24 h to 48 h in normal saline (0.9 wt% of aqueous solution of NaCl), as well as their size distribution. The increase in the hydrodynamic diameter of the GC/HA NP-5 was resulted from the fact that the introducing of salt partially reduces the electrostatic interaction between GC and HA.[40,41] More importantly, the GC/HA NP-5 still kept their spherical morphology and benign disperse state in normal saline, different from the polyelectrolyte multilayered capsules.[42] These results demonstrated that the GC/HA NP-5 could kept their spherical morphology with D_h less than 200 nm in various media, favorable for the prolonged circulation time in blood circulation and extravasation from blood stream into tumors through the EPR effect.

3.3. Surface charge-reversal

The zeta potentials of the GC/HA NP-5 varied from 19.70±0.50 mV to –40.47±1.96 mV as the media pH value changed from to 4.0 to 9.0 (Figure 4). When the media pH value was changed from 6.2 to 6.0, the zeta potential changed from -3.47±0.58 mV to 5.71±0.93 mV, interestingly indicating that the polyelectrolyte complex nanoparticles have the pH-dependent surface charge-reversal features in slightly acidic media mimicking the tumor extracellular environments, which may enhance cellular internalization in both *in vitro* and *in vivo*.[43]

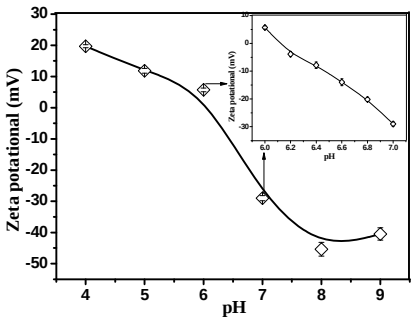

Figure 4. Zeta potentials of the GC/HA NPs (NP-5) in aqueous dispersions with different pH values. Zeta potential's value is shown (mean ± standard deviation, n=4).

The pH-dependent surface charge-reversal feature can be resulted from their unique "electrostatic sponge" structure. Both the protonation of GC and the deprotonation of HA increased the positive charge signal of the polyelectrolyte complex nanoparticles under such slightly acidic condition. It is well-known that CS is a weak polybase with the pKa value of about 6.5,[44] and HA is a weak polyacid with a *p*Ka value of about 3.2.[45] When the media pH was around 6.0, the zeta potential was 5.71± 0.93 mV, suggesting that the positively charge surpassed the negatively charge of the GC/HA NP-5 (Scheme 1). The similar phenomenon was found in their pH-stimuli responsive (Figure 3).This may be due to the protonation of GC at this pH, inducing the GC chains expanded and the positively charge exposed on surface of the GC/HA NP-5. As in the neutral and alkali media, the zeta potential of the GC/HA NP-5 was less than –29.00±0.81 mV, suggesting that the out shell was comprised of the deprotonated HA, while GC was collapsed and formed the inner complex cores (Scheme 1). As a potential DDS, this feature makes the polyelectrolyte complex nanoparticles maintain their stealth character during blood circulation and promote cellular uptake by tumor cells at the targeting tumor sites.

3.4. Drug loading and controlled release

To further explore the potential application of the GC/HA NP-5 in the drug release system, the positively charged DOX was used to evaluate the drug-loading capacity of the GC/HA NP-5. The negatively charged GC/HA NP-5 showed extremely high drug-loading efficiency (94.2%±1.8% (mean ± standard deviation, n=5)) and DOX-loading capacity (235.55 mg±4.51 mg/g (mean ± standard deviation, n=5)) at pH 7.4. Such high efficiency stemmed from the electrostatic interaction between the carboxyl groups of HA in the GC/HA NP-5 and the amine groups of DOX in the slightly alkali media (pH 7.4). Furthermore, the average hydrodynamic diameter (D_h) of the DOX-loaded GC/HA NP-5 increased to 198.3 ± 12 nm from 119 ± 5 nm of the GC/HA NP-5 with DLS at pH 5.0 (Figure 3Ac), and its zeta potential decreased to -21.23 ± 1.65 mV by compared with that of the GC/HA NP-5 (-38.47 ± 1.12 mv) at pH 7.4. The volume expansion and the

change in its surface charge indicated that DOX had been successfully encapsulated into the GC/HA NP-5 via the electrostatic interaction between the carboxyl groups of HA in the GC/HA NP-5 and the amine groups of DOX.

It is well known that the extracellular pH in normal tissues and blood is approximately 7.4 whereas in extracellular tumor tissues, the average pH is between 6.0 and 7.0 and drastically different acidic pH inside endosomes and lysosomes (pH 4.5–6.5).[46] Considering these pH differences, the DOX release was investigated subsequently under different physiological conditions (simulated body fluids at pH 7.4, 6.0, or 5.0) at 37 °C over a period of 34 h. The cumulative release ratio from the DOX-loaded GC/HA NP-5 reached 47.20 % at pH 6.0 within 270 min, while 46.13% at pH 5.0 within only 180 min. However, the cumulative release ratio was only 30% at pH 7.4 within 180 min. No burst release was observed in the three drug release system, mainly due to their unique "electrostatic sponge" structure. Interestingly, a significantly greater total release amount from the DOX-loaded GC/HA NP-5 at pH 5.0 (89.26%) was observed than that at pH 6.0 (69.74%), while only 51% at pH 7.4, revealing their pH-dependent manner: the release rate and cumulative amount of DOX increased as the pH value decreased (pH 5.0 > pH 6.0 > pH 7.4; Figure 5). The remarkable DOX release at acidic pH 5.0, and slightly acidic pH 6.0 was probably resulted from decrease in the electrostatic interaction between the GC/HA NP-5 and DOX,[7] as well as the increasing in the DOX solubility. The average hydrodynamic diameter (D_h) of the DOX-loaded GC/HA NP-5 increased to about 145 nm after drug-releasing at pH 5.0 PBS for 24 h (Figure 3Ab).

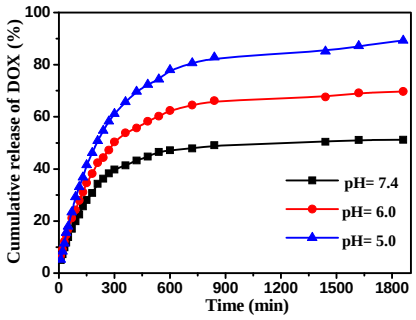

Figure 5. Cumulative DOX release in the simulated body fluids (pH 7.4, 6.0, and 5.0 at 37 °C) from the DOX-loaded GC/HA NP-5. Results show UV-vis analysis at room temperature at 480 nm for DOX. Each value represents the mean (SD <1%) (n=3).

A key feature of the GC/HA NP-5 is the negative-to-positive surface charge-reversal upon exposing to an acidic environment. With the acidity of the drug release system increasing, the surface charge of the GC/HA NP-5 changed from negative to positive. It means that the enhanced repulsive force between the positively charged GC/HA NP-5 and the positively charged DOX should contribute to the increase in the total release, due to that the electrostatic interaction between the GC/HA NP-5 and DOX is sensitive to the environmental pH value. The similar results was confirmed by the analysis of the zeta potentials and the pH stimulus-responsive properties of the GC/HA NP-5 via DLS.

The *in vitro* release kinetics of DOX was studied using the Higuchi and Korsmeyer-Peppas equations. Coefficients of correlation (R^2) were used to evaluate the fitting accuracy. The plots of Higuchi equation were used to described the DOX release mechanism from the DOX-loaded GC/HA NP-5 in simulated body fluids (pH 5.0, 6.0, or 7.4 at 37°C) (Figure S1 (a, c, and e)), showing linearity with R^2 and k value of 0.8485 and 2.2769, 0.8390 and 1.7242, 0.7960 and 1.2300, respectively. However, the linearity (R^2= 0.8485, 0.8390, and 0.7960) of the Higuchi equations leave much to be desired. So it could be concluded that diffusion was the primary governing force for the DOX releasing from the DOX-loaded GC/HA NP-5 in simulated body fluids (pH 5.0, 6.0 or 7.4 at 37 °C).[33]

As shown in Figure S1 (b, d, and f), the plots of Korsmeyer-Peppas equations resulted in linearity with the R^2 and the n value of 0.9240 and 0.5500, 0.9300 and 0.4000, 0.9161 and 0.4613 in simulated body fluids (pH 7.4, 6.0, or 5.0 at 37 °C), respectively. They yielded comparatively good linearity and release exponent of the approximately 0.5, indicating the release mechanism follows Fickian diffusion.[47] Both Higuchi and simplicity Korsmeyer-Peppas equations demonstrated that diffusion was the primary governing force for the drug release from the NP-5 in simulated body fluids.

3.5. Cell toxicity and hepatocyte-specificity assays

In vitro cytotoxicity of the DOX-loaded GC/HA NP-5 was evaluated with cultured HepG2 cells with MTT assays, with plain GC/HA NP-5 and free DOX as controls. As shown in Figure 6, the viability of the HepG2 cells was close to 100% within all the testing concentrations, meaning that the plain GC/HA NP-5 had little toxicity on the HepG2 cells in the given concentration range after 24 h incubation. More favorable cytocompatibility was found by increasing the concentration of the GC/HA NP-5 with cell viability of 99.7%±6.35%—103.1%±6.16% from 0 to 40μg/mL for 24 h. HepG2 cells are well-known model cells of parenchymal cells in the liver, hepatocytes, which have rich ASGP-R (asialoglycoprotein) receptors on the cell surface.[26] The DOX-loaded polyelectrolyte complex nanoparticles shown pronounced cytotoxic effect (Figure 6).[39]

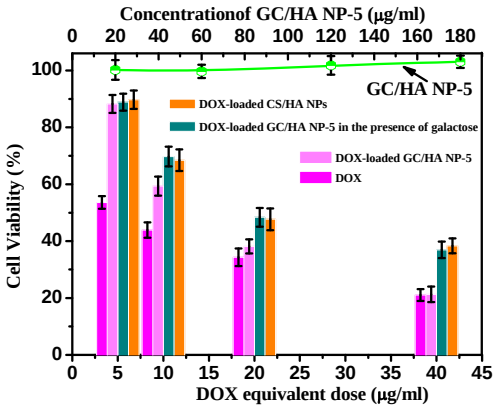

Figure 6. Cell viability assay in HepG2 cells. The cells were treated with GC/HA NPs, DOX-loaded CS/HA NPs, DOX-loaded GC/HA NP-5 in the presence of 1 mM lactobionic acid, DOX-loaded GC/HA NP-5 and free DOX at 37 °C for 24 h, respectively. Data are presented as the mean ± standard deviation (SD; n=5). Cell viability (%) was determined by the MTT assay.

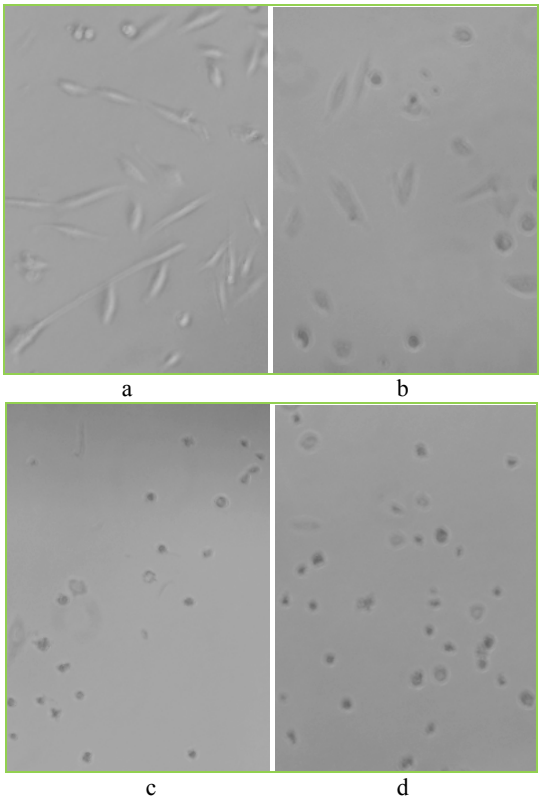

Figure 7. Typical micrographs of the HepG2 cells after incubation in the presence of (a) GC/HA NP-5, (b) DOX-loaded CS/HA NP-5, (c) DOX-loaded GC/HA NP-5, and (d) free DOX with the concentration (40 μg/mL) at 37 °C for 24 h.

To evaluate the galactose group mediated targeting function of the surface charge reversible GC/HA NP-5, the DOX-loaded GC/HA NP-5 and the DOX-loaded non-hepatocyte-specific CS/HA NP-5 were used for the in vitro study with HepG2 cells. Introducing DOX caused the reduction in cell viability and further decreased with increasing the DOX concentration (Figure 6). The order of efficacy as a killing agent was the free DOX, then the DOX-loaded GC/HA NP-5, and finally the DOX-loaded non-hepatocyte-specific CS/HA NP-5. Kim's group reported the single galactose-appended naphthalimide, which utilized galactose moiety as a hepatocyte-targeting unit to preferentially take up by HepG2 cells through galactose-targeted, ASGP-R-mediated endocytosis.[48] On the basis of above-mention discussion, the DOX-loaded GC/HA NP-5 were preferentially cellular uptake through galactose-targeted, ASGP-R-mediated endocytosis to release more DOX molecules to nucleus and further cause apoptosis of HepG2 cells.[49] Obviously, the GC/HA NP-5 have the favorable substitution values of galactose coupled with chitosan 50 k that is 5.91-6.13% of the total amine functions in chitosan by compared to the non-hepatocyte-specific CS/HA NP-5. The substitution values of galactose shows the high transfection in human hepatocyte derived cells lines (HepG2).[29] Meantime, the free lactobionic acid was introduced into comparative trial because of free lactobionic acid molecules would block the galactose group mediated targeting function. But even more crucial, the DOX-loaded GC/HA NP-5 in the presence 1 mM lactobionic acid present same inhibition effect to HepG 2 cells at the same scope of DOX equivalent dose by compared to DOX-loaded CS/HA NP-5. Taken together, the DOX-loaded hepatocyte-specific GC/HA NP-5 shown remarkable cell inhibition than the DOX loaded non-hepatocyte-specific GC/HA NP-5, mainly attributed to the ASGP-R receptors on the cell surface of the non-hepatocytes. This result indicated that the GC/HA NP-5 exhibited the receptor mediated hepatocyte specificity.

In addition, the morphologies of HepG2 cells treated with the GC/HA NP-5, DOX-loaded CS/HA NPs, DOX-loaded GC/HA NP-5, and free DOX are shown in Figure 7. Almost all HepG2 cells died in the case of the free DOX and the DOX-loaded GC/HA NP-5, while about 40% of the HepG2 cells survived with the DOX-loaded CS/HA NPs. It indicates that the DOX-loaded GC/HA NP-5 show remarkably cytotoxicity against HepG2 cells, showing the significant killing capability of the surface charge-reversible and specific hepatoma-targeting GC/HA NP-5 for hepatic tumor cells.

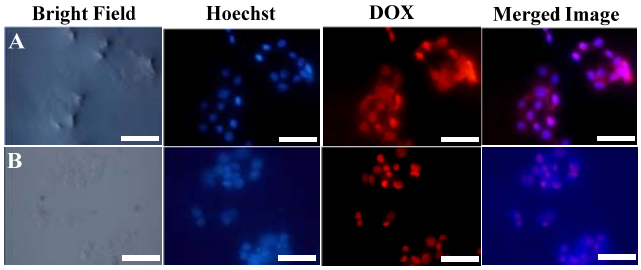

Figure 8. Cellular uptake of the DOX-loaded GC/HA NP-5 in the presence of 1 mM lactobionic acid (A) and DOX-loaded GC/HA NP-5 (B) exhibited by fluorescence microscope using HepG2 cells after a 12 h incubation. For each images, images from left to right show bright field, cell nuclei stained by Hoechst (blue), DOX fluorescence in cells (red), and merged images. The DOX equivalent dose having same concentration was 20 μg/mL, and the scale bar presented 50 μm.

3.6 Cellular uptake and galactose receptors (ASGP-R (asialoglycoprotein))-targeting for HepG2 cells

The cellular uptake of the DOX-loaded GC/HA NP-5 and galactose mediated targeting for HepG2 cells were evaluated through the fluorescence microscope as shown in Figure 8. It is worth noting that strong DOX red fluorescence is located in cell nuclei after 12 h incubation with the DOX-loaded GC/HA NP-5 in merge image, meaning the efficient cellular uptake of the DOX-loaded GC/HA NP-5 and remarkable intracellular release of loading DOX.[9] Compared with the DOX-loaded GC/HA NP-5, the DOX red fluorescence was located in external medium of HepG2 cells, and only partial DOX was detected in cell nuclei after 12 h incubation with the DOX-loaded GC/HA NP-5 in the presence of 1 mM free lactobionic acid. The higher cell uptake of DOX-loaded GC/HA NP-5 compared to that of DOX-loaded GC/HA NP-5 in the presence of 1 mM free lactobionic acid could be attributed to galactose-targeted, ASGP-R-mediated endocytosis. It indicated that the DOX-loaded GC/HA NP-5 presented notably targeting toward HepG2 cells, showing the significant DOX delivery for HepG2 cells from the DOX-loaded GC/HA NP-5. More importantly, owing to the recognition ability of the DOX-loaded GC/HA NP-5 was blocked,[50] the difference between the DOX-loaded GC/HA NP-5 in the presence of 1 mM free lactobionic acid and DOX-loaded GC/HA NP-5 were obviously observed. In addition, these results were further

evidenced with above MTT assays in Figure 6. Taking above exploration and analysis into consideration, the GC/HA NP-5 not only possessed pH-dependent surface charge-reversal feature, and higher DLC and DEE, but also had favorable biocompatibility and galactose-mediate targeting.

4. Conclusions

In summary, we have designed novel monodisperse pH-responsive surface charge-reversible and hepatoma-targeting GC/HA polyelectrolyte complex nanoparticles (GC/HA NPs) under mild condition at room temperature. As stable nanoparticles with D_h less than 200 nm in various simulated physiological media, their pH-dependent surface charge-reversal feature favors the stealth character during blood circulation and promote cellular uptake. The unique "electrostatic sponge" structure provides the GC/HA NPs higher DOX-loading capacity and the pH-triggering controlled release behaviour in simulated body fluids without burst release. They also show the outstanding biocompatibility and specific hepatoma-targeting due to the galactose-specific recognition of galactosylation of the GC and ASGR of hepatocytes. So the smart GC/HA NPs DDS prepared via a facile method with biodegradable polymers in the present work are expected to be potential for the cancer chemotherapy.

Acknowledgments

This project was granted financial support from and the "Chunhui Project" from the Ministry of Education of China (Grant no. Z2012116), the National Science Foundation for Fostering Talents in Basic Research of the National Natural Science Foundation of China (Grant No. J1103307), and the Innovation and Entrepreneurship Training Project for College Students from the Ministry of Education of China (Grant no. 201310730095).

Notes and references

[a] *State Key Laboratory of Applied Organic Chemistry and Key Laboratory of Nonferrous Metal Chemistry and Resources Utilization of Gansu Province, College of Chemistry and Chemical Engineering, Lanzhou University, Lanzhou 730000, China. Fax./Tel: 86 0931 8912582; E-mail: pliu@lzu.edu.cn.*

[b] *Department of Chemical Engineering, Monash University, VIC 3800, Australia*

1 R. D. Issels. *Eur. J. Cancer* **2008**, *44*, 2546.
2 R. de la Rica, D. Aili and M. M. Stevens. *Adv. Drug Delivery Rev.* **2012**, *64*, 967.
3 S. Kizaka-Kondoh, M. Inoue, H. Harada and M. Hiraoka. *Cancer Sci.* **2003**, *94*, 1021.
4 L. E. Gerweck and K. Seetharaman. *Cancer Res.* **1996**, *56*, 1194.
5 A. S. Narang and S. Varia. *Adv. Drug Delivery Rev.* **2011**, *63*, 640.
6 E. S. Lee, K. T. Oh, D. Kim, Y. S. Youn and Y. H. Bae. *J. Control Release* **2007**, *123*, 19.
7 J. Z. Du, T. M. Sun, W. J. Song, J. Wu and J. Wang. *Angew. Chem. Int. Ed.* **2010**, *49*, 3621.
8 X. L. Qiu, Q. L. Li, Y. Zhou, X. Y. Jin, A.D. Qi and Y.W. Yang. *Chem. Commun.* **2015**, *51*, 4237.
9 Q. L. Li, Y.F. Sun, Y. L. Sun, J. J. Wen, Y. Zhou, Q. M. Bing, L. D Isaacs, Y. H. Jin, H. Gao and Y. W. Yang. *Chem. Mater.* **2014**, *26*, 6418.
10 S. Ganta, H. Devalapally, A. Shahiwala and M. Amiji. *J. Control Release* **2008**, *126*, 187.
11 C. Deng, Y. J. Jiang, R. Cheng, F. H. Meng and Z. Y. Zhong. *Nano Today* **2012**, *7*, 467.
12 H. P. Xu, W. Cao and X. Zhang. *Acc. Chem. Res.* **2013**, *46*, 1647.
13 Z. S. Ge and S. Y. Liu. *Chem. Soc. Rev.* **2013**, *42*, 7289.
14 B. Law and C. H. Tung. *Bioconjug. Chem.* **2009**, *20*, 1683.
15 Y. L. Sun, Y. Zhou, Q. L. Li and Y. W. Yang. *Chem. Commun.* **2013**, *49*, 9033.
16 Y. Zhou, L. L. Tan, Q. L. Li, X. L. Qiu, A. D. Qi, Y. C. Tao and Y. W. Yang. *Chem. Eur. J.* **2014**, *20*, 2998.
17 N. Song and Y. W. Yang. *Chem. Soc. Rev.* **2015**, *44*, 3474.
18 H. Li, L.L. Tan, P. Jia, Q. L. Li, Y. L. Sun, J. Zhang, Y. Q. Ning, J. h. Yu and Y. W. Yang. *Chem. Sci.* **2014**, *5*, 2804.
19 V. Mailander and K. Landfester. *Biomacromolecules* **2009**, *10*, 2379.
20 S. E. Gratton, P. A. Ropp, P. D. Pohlhaus, J. C. Luft, V. J. Madden, M. E. Napier and J. M. DeSimone. *Proc. Natl. Acad. Sci. USA* **2008**, *105*, 11613.
21 E. C. Cho, J. Xie, P. A. Wurm and Y. Xia. *Nano Lett.* **2009**, *9*, 1080.
22 D. Oupicky, M. Ogris, K. A. Howard, P. R. Dash, K. Ulbrich and L. W. Seymour. *Mol. Ther.* **2002**, *5*, 463.
23 Y. Lee, T. Ishii, H. Cabral, H. J. Kim, J.-H. Seo, N. Nishiyama, H. Oshima, K. Osada and K. Kataoka. *Angew. Chem. Ed. Int.* **2009**, *48*, 5309.
24 J. A. MacKay, M. Chen, J. R. McDaniel, W. Liu, A. J. Simnick, A. Chilkoti. *Nature Mater.* **2009**, *8*, 993.
25 W. P. Gao, W. G. Liu, T. Christensen, M. R. Zalutsky and A. Chilkoti. *Proc. Natl. Acad. Sci. USA* **2010**, *107*, 16432.
26 J. H. Park, L. Gu, G. von Maltzahn, E. Ruoslahti, S. N. Bhatia and M. J. Sailor. *Nature Mater.* **2009**, *8*, 331.
27 Hobbs, S. K.; Monsky, W. L.; Yuan, F.; Roberts, W. G.; Griffith, L.; Torchilin, V. P.; Jain, R. K. . *Proc. Natl. Acad. Sci. USA* **1998**, *95*, 4607.
28 S. R. MacEwan, D. J. Callahan and A. Chilkoti. *Nanomedicine (Lond)* **2010**, *5*, 793.
29 J. M. Rosenholm, A. Meinander, E. Peulhu, R. Niemi, J. E. Eriksson, C. Sahlgren and M. Linden. *ACS Nano 2009*, **3**, 197.
30 T. H. Kim, I. K. Park, J. W. Nah, Y. J. Choi and C. S. Cho. *Biomaterials* **2004**, *25*, 3783.
31 X. B. Zhao and P. Liu. *Mol. Pharmaceutics* **2014**, *11*, 1599.
32 P. Liu and X. B. Zhao. *Biotechnol. J.* **2013**, *8*, 847.
33 T. Higuich. *J. Pharm. Sci.* **1961**, *50*, 874.
34 R. W. Korsmeyer, R. Gurny, E. M. Doelker, P. Buri and N. A. Peppas. *Int. J. Pharm.* **1983**, *15*, 25.
35 T. Bettinger, J. S. Remy and P. Erbacher. *Bioconjug. Chem.* **1999**, *10*, 558.
36 Y. Chen, D. Ding, Z. Q. Mao, Y. F. He, Y. Hu, W. Wu and X. Q. Jiang. *Biomacromolecules* **2008**, *9*, 2609.
37 C. L. de Vasconcelos, P. M. Bezarril, D. E. S. dos Santos, T. N. C. Dantas, M. R. Pereira and J. L. C. Fonseca. *Biomacromolecules* **2006**, *7*, 1245.
38 Y. Hu, M. T. Yang and X. M. Hu, *Polym. Bull.* **2012**, *68*, 1183.
39 X. Z. Shu, K. J. Zhu and W. Song. *Int. J. Pharm.* **2001**, *212*, 19.
40 X. B. Zhao, P. C. Du and P. Liu. *Mol. Pharmaceutics* **2012**, *9*, 3330.
41 T. Govender, S. Stolnik, C. Xiong, S. Zhang, L. Illum and S. S. Davis. *J. Control Release* **2001**, *75*, 249.
42 P. Liu. *Adv. Colloid Interface Sci.* **2014**, *207*, 178.
43 V. Mailander and K. Landfester. *Biomacromolecules* **2009**, *10*, 2379.
44 A. L. Hillberg and M. Tabrizian. *Biomacromolecules* **2006**, *7*, 2742.
45 Y. X. Zhu and S. Granick. *Macromolecules* **2003**, *36*, 973.
46 R. F. Murphy, S. Powers and C. R. Cantor. *J. Cell Biol.* **1984**, *98*, 1757.
47 A. Raval, J. Parikh and C. Engineer. *Ind. Eng. Chem. Res.* **2011**, *50*, 9539.
48 M. H. Lee, J. H. Han, P. Kwon, S. Bhuniya, J. Y. Kim, J. L. Sessler, C. Kang and J. S. Kim. *J. Am. Chem. Soc.* **2012**, *134*, 1316.
49 X. B. Zhao and P. Liu. *ACS Appl. Mater. Interfaces* **2015**, *7*, 166.
50 J. L. Lv, H. L. Sun, Y. Zou, F. H. Meng, A. Dias, M. Hendriks, J. Feijena and Z. Y. Zhong. *Biomater. Sci.* **2015**, *3*, 1134.

Graphical Abstract